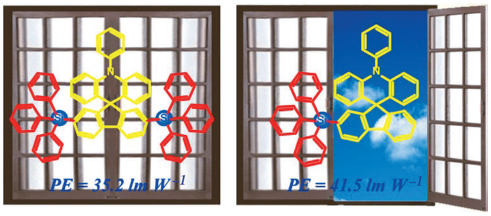

Into the blue: Blue phosphorescent material 10-phenyl-2′-(triphenylsilyl)-10*H*-spiro[acridine-9,9′-fluorene] (SSTF) has been synthesized. The triphenylsilyl side group imparts good thermal stability. The energy levels of SSTF make it suitable as a host material or exciton-blocking layer in blue phosphorescent organic light-emitting diodes (see figure; PE = power efficiency).

Phosphorescence

H. Chen, Z.-Q. Jiang, C.-H. Gao, M.-F. Xu, S.-C. Dong, L.-S. Cui, S.-J. Ji,* L.-S. Liao* .... ▮▮▮▮–▮▮▮▮

Silicon-Based Material with Spiro-Annulated Fluorene/Triphenylamine as Host and Exciton-Blocking Layer for Blue Electrophosphorescent Devices

DOI: 10.1002/chem.201301106

Silicon-Based Material with Spiro-Annulated Fluorene/Triphenylamine as Host and Exciton-Blocking Layer for Blue Electrophosphorescent Devices

Hua Chen,[a] Zuo-Quan Jiang,*[b] Chun-Hong Gao,[b] Mei-Feng Xu,[b] Shou-Cheng Dong,[b] Lin-Song Cui,[b] Shun-Jun Ji,*[a] and Liang-Sheng Liao[b]

Abstract: A novel silicon-based compound, 10-phenyl-2′-(triphenylsilyl)-10*H*-spiro[acridine-9,9′-fluorene] (SSTF), with spiro structure has been designed, synthesized, and characterized. Its thermal, electronic absorption, and photoluminescence properties were studied. Its energy levels make it suitable as a host material or exciton-blocking material in blue phosphorescent organic light-emitting diodes (PhOLEDs). Accordingly, blue-emitting devices with iridium(III) bis[(4,6-difluorophenyl)-pyridinato-*N*,$C^{2'}$]picolinate (FIrpic) as phosphorescent dopant have been fabricated and show high efficiency with low roll-off. In particular, 44.0 cd A^{-1} (41.3 lm W^{-1}) at 100 cd m^{-2} and 41.9 cd A^{-1} (32.9 lm W^{-1}) at 1000 cd m^{-2} were achieved when SSTF was used as host material; 28.1 lm W^{-1} at 100 cd m^{-2} and 20.6 lm W^{-1} at 1000 cd m^{-2} were achieved when SSTF was used as exciton-blocking layer. All of the results are superior to those of the reference devices and show the potential applicability and versatility of SSTF in blue PhOLEDs.

Keywords: electrophosphorescence · host–guest systems · luminescence · organic light-emitting diodes · spiro compounds

Introduction

A rapid growth of organic light-emitting diode (OLED) technology, commercialized in small flat-panel displays, cell phones, cameras, and solid-state lighting, has been witnessed in recent years.[1,2] Meanwhile, fundamental organic materials research on OLEDs has also been dramatically developed to meet the daily-increasing demand. In the development of OLED materials, phosphorescent materials have attracted tremendous attention because of their capability of harvesting both the singlet and triplet excitons, since the pioneering work in 1998.[3,4] The large spin–orbital coupling of the heavy metals (Ir, Pt, or Os etc.) leads to an efficient intersystem crossing and thus to a theoretical internal quantum efficiency as high as 100 %. The high-efficiency emitter, however, cannot be utilized directly as a single emitting layer because of its almost inevitable triplet–triplet annihilation and triplet–polaron annihilation of triplet-state excitons at high concentration, which originates from its intrinsic long lifetime of phosphorescence. An effective way to solve the problem is by adopting a host matrix to separate the metal complex.[5–10] Therefore, synthesizing good host materials is another important issue as well as seeking good guest emitters.[11–22]

The first principle for designing good host materials is impeding reverse energy transfer from the guest to the host and confining the exciton in the emitting layer.[23] Under this guideline, many materials have been prepared and one of the prominent classes is silicon-based compounds. In 2004, Ren et al. first reported a series of host materials, including 1,4-bis(triphenylsilyl)benzene (UGH) (Scheme 1), with ultrawide energy gap;[24] in 2008, Lin et al. prepared bis-styrylbenzene (BSB) with the aim to increase the conductivity of UGH.[25] Note that these types of materials could also easily fulfill the second principle for designing host materials: forming stable amorphous films.[26] This property guarantees that the emitter stays uniformly diluted in the matrix to minimize the effect of concentration quenching. As a bulky group, tetraphenylsilane could play a major role in avoiding strong intermolecular aggregation.[27] The third principle for designing good host materials is a suitable HOMO and LUMO for charge transfer and injection. Due to the high injection barrier in UGH and BSB resulting from their deep HOMO levels, the performances are relatively low though they can meet the aforementioned two principles. The solution is to introduce electron-active moieties, and in this way, many host materials have been developed in the past few years.

---

[a] H. Chen, Prof. Dr. S.-J. Ji
Key Laboratory of Organic Synthesis of Jiangsu Province
College of Chemistry, Chemical Engineering, and Materials Science
Soochow University, Suzhou 215123 (P. R. China)
Fax: (+86) 0512-65880307
E-mail: shunjun@suda.edu.cn

[b] Prof. Dr. Z.-Q. Jiang, C.-H. Gao, M.-F. Xu, S.-C. Dong, L.-S. Cui,
Prof. Dr. L.-S. Liao
Jiangsu Key Laboratory for
Carbon-Based Functional Materials & Devices
Institute of Functional Nano & Soft Materials (FUNSOM)
Soochow University, Suzhou 215123 (P. R. China)
Fax: (+86) 0512-65882846
E-mail: zqjiang@suda.edu.cn

Supporting information for this article is available on the WWW under http://dx.doi.org/10.1002/chem.201301106.

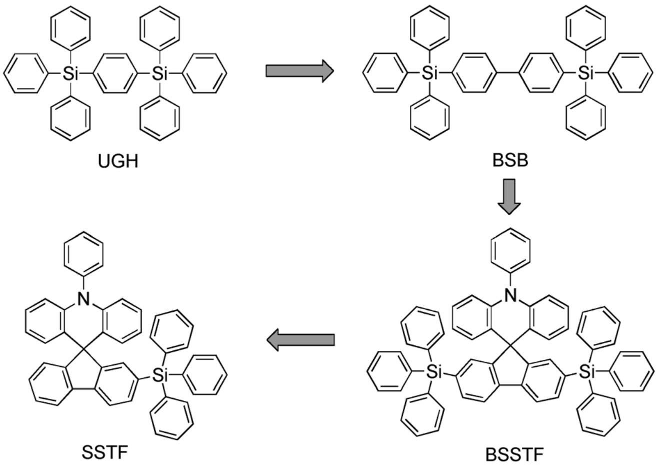

Scheme 1. Chemical structures of materials employed.

For example, Kang et al. synthesized 9-(4-triphenylsilanyl-(1,1′,4,1″)-terphenyl-4″-yl)-9*H*-carbazole by replacing one triphenylsilyl group of BSB with *N*-carbazole, but its triplet energy drops steeply to 2.4 eV, which means it is unsuitable for blue phosphorescence.[28] Yeh et al. added a triphenylsilyl group to the conventional blue host *N*,*N*′-dicarbazolyl-3,5-benzene (mCP) (e.g., SimCP) to improve its thermal stability and achieved a power efficiency of 11.9 lm W^{-1}.[29] Tsai et al. developed 9-(4-*tert*-butylphenyl)-3,6-bis(triphenylsilyl)-9*H*-carbazole by appending two triphenylsilyl groups on the *para* positions of phenyl-9*H*-carbazole, which achieved a power efficiency of 26.7 lm W^{-1}.[30] Han et al. developed a series of tetrahedral silicon motifs with carbazole, and the best performance was 13.6 lm W^{-1}.[31] Jiang et al. proposed that the bridged triphenylamine may be a good candidate for blue host materials, and the afforded bridged triphenylamine triphenylsilane (BTPASi) with two triphenylsilyl groups showed a power efficiency of 35 lm W^{-1}.[32] Leung et al. used electron-deficient oxadiazole containing silane to construct an n-type host, and the maximum power efficiency was 31.4 lm W^{-1}.[33] Gong et al. used the tetraphenylsilane as a bridge to link diphenylamine and benzimidazole groups (e.g., *p*-BISiTPA), and this material displayed a power efficiency of 26.1 lm W^{-1} and low-efficiency roll-off.[34]

Herein, we describe a successful combination of a high triplet energy moiety based on the BSB molecule and the triphenylamine moiety through spiro-annulated linkage to give 10-phenyl-2′,7′-bis(triphenylsilyl)-10*H*-spiro[acridine-9,9′-fluorene] (BSSTF; Scheme 1). This structure possesses the triphenylamine as hole-transport group with high triplet energy[35] and the 3D cardo moiety to improve thermal stability to form the amorphous glassy state;[36–38] the nonconjugated expansion in size retained the high triplet energy of BSB. In general, we suppose that these aspects will comply well with the requirements of good host materials. After this initial molecular design, we speculated that it might not be necessary to append two triphenylsilyl groups on BSSTF and we subsequently subtracted one of them to obtain a monosubstituted analogue 10-phenyl-2′-(triphenylsilyl)-10*H*-spiro[acridine-9,9′-fluorene] (SSTF) with an asymmetric conformation. As a result, efficient blue phosphorescent devices employing the new host materials have been fabricated. The device with BSSTF as host shows a maximum current efficiency of 41 cd A^{-1} (35.2 lm W^{-1}). This performance is quite good relative to previous work. Additionally, the device with SSTF as host exhibits an even lower turn-on voltage of 3.3 V and higher maximum current efficiency of 44.0 cd A^{-1} (41.5 lm W^{-1}). Remarkably, a rather low roll-off value of 4.8 % is observed in this device at a practical luminance of 1000 cd m^{-2}. To the best of our knowledge, this is among the highest performances for iridium(III) bis[(4,6-difluorophenyl)-pyridinato-*N*,*C*$^{2'}$]picolinate (FIrpic)-based phosphorescent OLEDs (PhOLEDs) accompanied by such low-efficiency roll-off. Furthermore, we found that the SSTF can also act as a good exciton-blocking material in PhOLEDs and we compared it with the traditional exciton materials (1,1-bis[(di-4-tolylamino)phenyl]cyclohexane (TAPC), 4,4′,4″-tris(*N*-carbazolyl)triphenylamine (TCTA), and mCP) to reveal its versatile and superior application in this research area.

Results and Discussion

Synthesis: The synthetic route is outlined briefly in Scheme 2. According to the literature, we first synthesized the precursors **1** and **2** by treating bromotriphenylamine with *n*BuLi at −78 °C, then adding 2-bromo-9,9′-spirobifluorene or 2,7-dibromo-9,9′-spirobifluorene, following Friedel–Crafts cyclization to afford good yields.[39] Subsequently, the novel materials BSSTF and SSTF were synthesized from these precursors by a one-step reaction through lithium–halogen exchange then quenching with triphenylchlorosilane. Compared with BSSTF, the SSTF has a smaller molecular size and may be more suitable for vapor deposition in device fabrication. Their chemical structures were fully char-

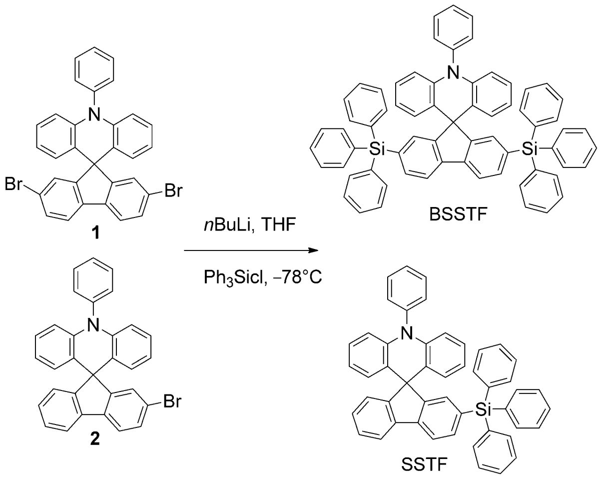

Scheme 2. Synthetic route of materials employed.

acterized by ^{1}H and ^{13}C NMR spectroscopy, mass spectrometry, and elemental analysis.

Thermal properties: We investigated the thermal stabilities of the compounds by thermogravimetric analysis (TGA) and differential scanning calorimetry (DSC) in a nitrogen atmosphere at a scanning rate of 10 °C min^{-1}. Both the materials exhibited high thermal decomposition temperatures (T_d, corresponding to 5 % weight loss, see Figure 1): 458 °C for BSSTF and 327 °C for SSTF. Their glass transition temperatures T_g were observed at 134 °C for BSSTF and 109 °C for SSTF, which are substantially higher than those of traditional host materials, such as 4,4′-bis(9-carbazolyl)biphenyl (CBP) (62 °C) and mCP (60 °C). As we know, a bigger analogue always results in relatively higher T_d and T_g values, and these results are not beyond our preliminary design. The rigid spiro structure of the new materials always leads to good thermal characteristics, and the triphenylsilyl side group can effectively avoid strong intermolecular packing to form stable amorphous films.

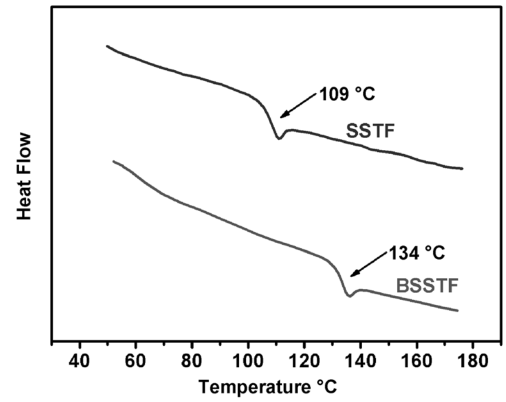

Figure 1. DSC traces recorded at a heating rate of 10 °C min^{-1}.

Ultraviolet photoelectron spectroscopy: The ionization potentials (IPs) of the host materials were measured by using ultraviolet photoelectron spectroscopy (UPS). This technique determines the HOMO energy level in organic thin films by bombarding the sample with UV photons and measuring the kinetic energies of the ejected valence electrons. Thus, the HOMO values obtained by this technique are very precise relative to the more commonly used technique of cyclic voltammetry (CV), which requires the use of approximations and has a high degree of error associated with the measurements (> 0.1 eV). The IPs for BSSTF and SSTF are 5.67 and 5.66 eV, respectively. These values are nearly identical, which means that the difference of substitution paths did not affect the electron distribution of the HOMOs, because the HOMOs are mainly distributed on the triphenylamine parts as expected. For comparison, we also tested their electrochemical behavior by CV. The same oxidation onsets also determined that they have similar HOMO energy levels, but values of 5.35 eV for BSSTF and 5.33 eV for SSTF, which were quite different from the results from UPS (Figure S9, Supporting Information).

Photophysical properties: BSSTF and SSTF also show almost the same electronic absorption, for example, 280 nm for BSSTF and 273 nm for SSTF (Figure 2), thus indicating that the absorption could be attributed to the π–π* transition of their common spiro-triphenylamine/fluorene core. Their photoluminescence (PL) spectra in CH_2Cl_2 solution depict that the BSSTF has a larger Stokes shift than SSTF, which may account for the vibration relaxation of the two triphenylsilyl side groups of BSSTF. The phosphorescence spectra of BSSTF and SSTF (Figure 2) were measured in a frozen 2-methyltetrahydrofuran (2-MeTHF) matrix at 77 K. The energy gaps determined by the onset of UV/Vis spectra and the triplet energies calculated from the first peak of the phosphorescence spectra indicate that the SSTF has a slightly higher singlet energy gap (3.81 > 3.78 eV) and triplet energy (2.81 > 2.76 eV). Their geometrical and electronic properties were further studied by density functional theory (DFT) calculations using the B3LYP hybrid functional. From the computer simulation, we found that the triphenylsilyl group exerted little effect on the distributions on HOMOs, LUMOs, and localized spin densities of the T1 states for BSSTF and SSTF; the tendency of the calculated results also correlated well with the measurements (Figures S10 and S11, Supporting Information). These data, as well as the electron affinities (EAs) calculated from the optical bandgaps and the IPs measured by UPS, are summarized in Table 1.

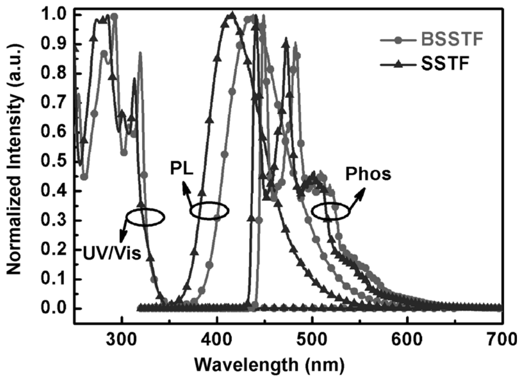

Figure 2. UV/Vis absorption and PL spectra measured in dichloromethane solution at 10^{-5} M; phosphorescence (Phos) spectra measured in frozen 2-methyltetrahydrofuran matrix at 77 K.

Electroluminescence performance: In light of the high triplet energies of the novel materials, blue electrophosphorescent devices with BSSTF and SSTF as host materials and mCP as reference were fabricated. The device structure was ITO/HAT-CN (10 nm)/TAPC (45 nm)/host FIrpic 15 wt % (20 nm)/TmPyPB (40 nm)/Liq (2 nm)/Al (100 nm), in which ITO = indium tin oxide, HAT-CN = dipyrazino[2,3-f:2′,3′-h]quinoxaline-2,3,6,7,10,11-hexacarbonitrile, TmPyPB =

Table 1. Physical properties of BSSTF and SSTF.

	T_g[a] [°C]	T_d[a] [°C]	$\lambda_{max,abs}$[b] [nm]	$\lambda_{max,f}$[b] [nm]	λ_{ph}[c] [nm]	E_g[d] [eV]	E_T/IP/EA[e] [eV]	E_T/IP/EA[f] [eV]
BSSTF	134	458	292, 319	437	449	3.78	2.76/5.67/1.89	2.92/5.28/1.37
SSTF	109	327	285, 313	413	440	3.81	2.81/5.66/1.85	2.98/5.31/1.31

[a] T_g: glass transition temperature, T_d: decomposition temperature; measured by DSC and TGA. [b] Measured in dichloromethane solution at room temperature. [c] Measured in 2-MeTHF glass matrix at 77 K. [d] E_g: the bandgap energies were estimated from the optical absorption edges of UV/Vis absorption spectra. [e] E_T: the triplet energies were estimated from the onset peak of the phosphorescence spectra; IP and EA were calculated from UPS and the optical bandgaps from the absorption spectra. [f] E_T, IP, and EA were calculated from DFT simulations.

1,3,5-tri(*m*-pyrid-3-yl-phenyl)benzene), and Liq = 8-hydroxyquinolatolithium. HAT-CN and Liq were used as hole-injection and electron-injection layers, respectively, TAPC was used as hole-transporting layer, and TmPyPB served as electron-transporting layer; the emitting material consisted of FIrpic doped in host materials mCP (Device 1), BSSTF (Device 2), or SSTF (Device 3). All the devices showed identical spectra from the guest FIrpic without any emission from the host and/or adjacent layer, thus indicating that the excitons were entirely confined in the emitting layer. All device characteristics are summarized in Table 2. The reference Device 1 obtained a maximum current efficiency of 34.5 cd A^{-1}, a maximum power efficiency of 23.2 lm W^{-1}, and a maximum external quantum efficiency of 13.7 % with turn-on voltage of 4.2 V at 100 cd m^{-2} (Figures 3 and 4). Both Device 2 and Device 3 exhibited better performance than Device 1. For example, Device 2 achieved a maximum current efficiency of 41.0 cd A^{-1}, a maximum power efficiency of 35.2 lm W^{-1}, and a maximum external quantum efficiency of 17.4 %. On the other hand, it is noticeable that the driving voltages of Device 2 (3.7 V) and Device 3 (3.3 V) met the requirement for portable display (< 4 V at 100 cd m^{-2}). In addition, Device 3 presented not only the highest efficiency and the lowest driving voltage of all the devices, but also a very low efficiency roll-off in device operation. The maximum current efficiency of Device 3 was 44.0 cd A^{-1}, corresponding to a power efficiency of 41.5 lm W^{-1} and an external quantum efficiency of 18.7 %; the current efficiency roll-off, notably, was just 4.8 % at a luminance of 1000 cd m^{-2} (Figure 3). In general, the performance (41.9 cd A^{-1} and 32.9 lm W^{-1}) and the efficiency roll-off (4.8 %) of Device 3 at the practical lighting brightness of 1000 cd m^{-2} are, to the best of our knowledge, the best among the blue PhOLEDs with FIrpic as guest emitter.

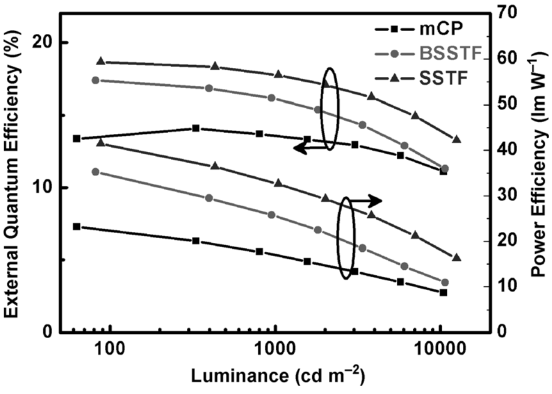

Figure 3. Current efficiency and power efficiency versus luminance for Devices 1–3.

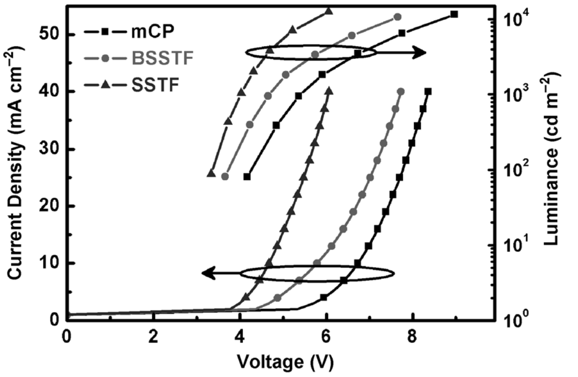

Figure 4. Current density and luminance versus voltage for Devices 1–3.

To further understand the difference in the device performance with BSSTF or SSTF as host material, we fabricated hole-only devices with a structure of ITO/MoO_3 (10 nm)/host (100 nm)/MoO_3 (10 nm)/Al (100 nm). The MoO_3 layer was utilized to prevent electron injection from the cathode, which could be ascribed to the large electron-injection barrier between the MoO_3 (LUMO = 2.3 eV) and Al (4.3 eV) layers. From this measurement, we found that the SSTF presented the highest hole mobility among the three host materials (Figure 5). On comparing BSSTF with SSTF, the bigger interference by the more substituted triphenylsilyl groups of

Table 2. Electroluminescence characteristics of devices 1–3.

Host	V_{on}[a] [V]	$\eta_{c.max}$[b] [cd A^{-1}]	η_c@100 cd m^{-2} [cd A^{-1}]	η_c@1000 cd m^{-2} [cd A^{-1}]	$\eta_{p.max}$[c] [lm W^{-1}]	η_p@100 cd m^{-2} [lm W^{-1}]	η_p@1000 cd m^{-2} [lm W^{-1}]	$\eta_{ext.max}$[d] [%]	CIE[e] (*x*,*y*)
mCP	4.2	34.5	34.3	32.1	23.2	22.7	17.1	13.7	0.167, 0.366
BSSTF	3.7	41.0	40.9	38.0	35.2	34.9	25.5	17.4	0.162, 0.364
SSTF	3.3	44.0	44.0	41.9	41.5	41.3	32.9	18.7	0.161, 0.364

[a] Turn-on voltage at 100 cd m^{-2}. [b] Maximum current efficiency. [c] Maximum power efficiency. [d] Maximum external quantum efficiency. [e] Commission Internationale de l'Éclairage coordinates measured at 5 mA cm^{-2}.

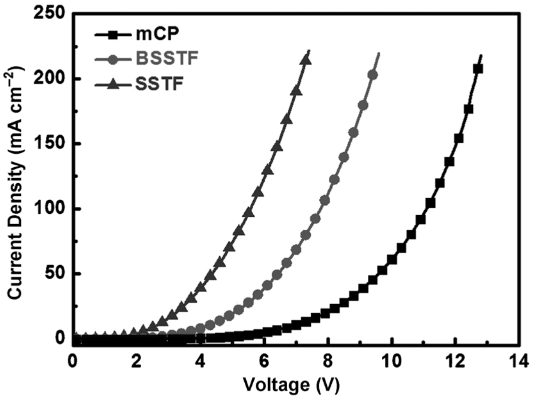

Figure 5. Current density–voltage (*J*–*V*) curves for the hole-only devices (ITO/MoO_3 (10 nm)/mCP, BSSTF or SSTF (100 nm)/MoO_3 (10 nm)/Al (100 nm).

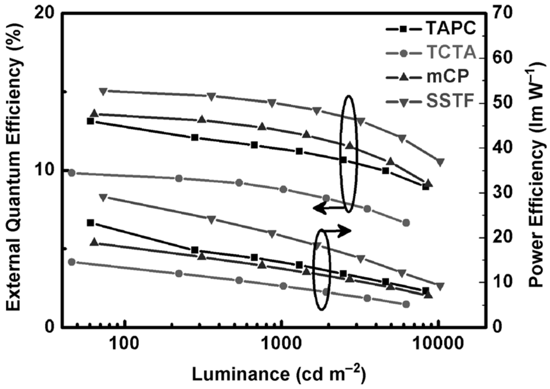

Figure 6. Current efficiency and power efficiency versus luminance for devices with different EBLs.

BSSTF may hamper the carrier hopping from one molecule to a neighboring molecule and thus lead to lower mobility. The tendency for hole mobility agreed well with the corresponding device performance. We also made electron-only devices with a structure of ITO/TmPyPB (20 nm)/mCP, BSSTF or SSTF (100 nm)/TmPyPB (20 nm)/Liq (2 nm)/Al (100 nm), and the hole-only current densities (*J*) of SSTF and BSSTF were about two orders of magnitude bigger than the electron-only *J* values, which indicated negligible electron transport in SSTF and BSSTF (see the Supporting Information). Considering that BSSTF and SSTF possessed very similar HOMO/LUMO levels and triplet energies, the higher hole mobility may account for the lower driving voltage and better performance of the SSTF-based device.

Considering its high hole-transporting mobility, wide triplet energy level, suitable HOMO/LUMO levels, and good thermal stability, SSTF could also act as an exciton-blocking layer (EBL) for which the traditional materials, such as TAPC, TCTA, and mCP, are always used in blue phosphorescent devices. In this kind of device structure, the EBL is used to prevent excitons diffusing out of the emitting layer and energy back-transfer from the triplet level of FIrpic to the adjacent hole-transporting layer, typically if the hole-transporting material features a low triplet energy (such as the ubiquitous material 4,4′-bis[*N*-(1-naphthyl)-*N*-phenylamino]biphenyl (NPB)). The fundamental features of SSTF are similar to those of commonly used exciton-blocking materials, so we fabricated a prototype device with the structure ITO/HAT-CN (10 nm)/NPB(80 nm)/EBL (15 nm)/mCP:FIrpic 8 wt% (20 nm)/TmPyPB (40 nm)/Liq (2 nm)/Al (100 nm), in which EBL = TAPC, TCTA, mCP, or SSTF, to evaluate their performance. Satisfactorily, the SSTF-based device also showed the best performance in this kind of blue phosphorescent device with a maximum current efficiency of 36.5 cd A^{-1}, a maximum power efficiency of 29.1 lm W^{-1}, and a maximum external quantum efficiency of 15.1% (Figure 6, Table 3). Especially at an applied brightness of 1000 cd m^{-2}, the SSTF-based device showed a superior performance to that of the others (Figure 7). The power efficiency of SSTF presented 42 and 60% improvement relative to that of TAPC and mCP, respectively, and had more than twice the power efficiency of TCTA.

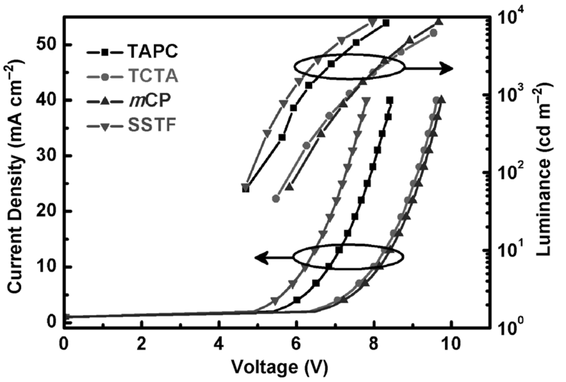

Figure 7. Current density and luminance versus voltage for devices with different EBLs.

Table 3. Electroluminescence characteristics of the devices with different EBLs.

Host	V_{on}[a] [V]	$\eta_{c.max}$[b] [cd A^{-1}]	η_c@100 cd m^{-2} [cd A^{-1}]	η_c@1000 cd m^{-2} [cd A^{-1}]	$\eta_{p.max}$[c] [lm W^{-1}]	η_p@100 cd m^{-2} [lm W^{-1}]	η_p@1000 cd m^{-2} [lm W^{-1}]	$\eta_{ext.max}$[d] [%]	CIE[e] (*x*,*y*)
TAPC	4.5	30.5	29.8	26.4	23.2	21.2	14.5	13.1	0.168, 0.355
TCTA	5.4	23.0	22.5	20.6	14.5	13.3	9.2	9.8	0.169, 0.356
mCP	5.6	32.0	31.7	29.6	18.8	17.9	12.9	13.6	0.169, 0.361
SSTF	4.2	36.5	36.4	34.5	29.1	28.1	20.6	15.1	0.173, 0.377

[a] Turn-on voltage at 100 cd m^{-2}. [b] Maximum current efficiency. [c] Maximum power efficiency. [d] Maximum external quantum efficiency. [e] Commission Internationale de l’Éclairage coordinates measured at 5 mA cm^{-2}.

Conclusion

We have synthesized and characterized two materials, BSSTF and SSTF, and their morphological stability, triplet energy (E_T), and HOMO/LUMO energy levels have been investigated. On application in blue phosphorescent devices, the asymmetric material SSTF showed better performance with a power efficiency of 41.5 lm W^{-1} and a current efficiency of 44 cd A^{-1} with efficiency roll-off of 4.8 % at the practical brightness of 1000 cd m^{-2}. These values are among the highest levels in the scientific literature and represent the successful design of the silicon-based host material to date. We also fabricated another kind of blue PhOLED with SSTF as EBL. It is encouraging to find that its performance is superior to those of traditional materials, such as TAPC, TCTA, and mCP. Our results showed that SSTF may be a promising candidate for high-efficiency blue PhOLEDs.

Experimental Section

Device fabrication and measurement: OLED devices were fabricated on 0.7-mm-thick glass substrates precoated with a transparent ITO conductive layer with a thickness of approximately 100 nm and a sheet resistance of approximately 30 Ω per square. The substrates, after being cleaned, dried, and treated by UV/ozone successively, were transferred into a vacuum chamber for sequential deposition of all organic and metal layers on top of the substrates in a vacuum of approximately 2×10^{-6} Torr. The deposition rates and doping concentrations of materials were controlled and measured in situ by using calibrated thickness monitors. After the deposition of all layers, four identical OLEDs were formed on each of the substrates, and each OLED had an emission area of 0.1 cm^2. The electroluminescence characteristics of all the devices were evaluated by using a Keithley 2400 SourceMeter constant-current source and a Photo Research SpectraScan PR 655 photometer at room temperature. The external quantum efficiency values were calculated according to previously reported methods. All measurements were carried out at room temperature under ambient conditions.

Synthesis of materials: Compound **1** or **2** was dissolved in THF under argon and cooled to −78 °C. *n*-Butyllithium was added dropwise to the solution under vigorous stirring. After reaction at −78 °C for 1 h, a solution of chlorotriphenylsilane in THF was added dropwise. The resulting mixture was stirred at −78 °C for 1 h, and then gradually warmed to room temperature. After stirring overnight, water (5 mL) was added. Then the mixture was evaporated, extracted with dichloromethane, and washed with water successively. The organic layer was collected, dried with Na_2SO_4, filtered, and evaporated. The crude product was purified by column chromatography on silica gel.

BSSTF (10-phenyl-2′,7′-bis(triphenylsilyl)-10H-spiro[acridine-9,9′-fluorene]): Compound **1** (1.70 g, 3 mmol), *n*-butyllithium (2.4 M, 9 mmol), and chlorotriphenylsilane (3.54 g, 12 mmol) were employed. Petroleum ether/ethyl acetate (6:1, v/v) was used as eluent for column chromatography. The final product was a white powder (1.78 g, 64.1 %). ^{1}H NMR (400 MHz, $CDCl_3$): δ = 7.90 (s, 2 H), 7.77 (d, J = 7.6 Hz, 2 H), 7.55–7.52 (s, 1 H), 7.51–7.45 (m, 13 H), 7.44–7.39 (m, 4 H), 7.37 (dt, J = 2.7, 1.8 Hz, 5 H), 7.29 (t, J = 7.2 Hz, 12 H), 6.91 (dd, J = 8.5, 7.1, 1.6 Hz, 2 H), 6.75 (dd, J = 6.4, 3.1 Hz, 2 H), 6.68–6.60 (m, 2 H), 6.57 (dd, J = 7.7, 1.5 Hz, 2 H), 6.18 ppm (d, J = 7.6 Hz, 2 H); ^{13}C NMR (100 MHz, $CDCl_3$): δ = 154.54, 141.58, 140.56, 140.47, 136.37, 135.80, 134.44, 134.21, 133.73, 130.99, 130.77, 129.51, 127.92, 127.82, 127.03, 126.47, 125.08, 120.34, 119.86, 114.39, 57.24 ppm; MS: *m/z*: 923.34; elemental analysis calcd (%) for $C_{67}H_{49}NSi_2$: C 87.06, H 5.34, N 1.52; found: C 87.00, H 5.35, N 1.77.

SSTF (10-phenyl-2′-(triphenylsilyl)-10H-spiro[acridine-9,9′-fluorene]): Compound **2** (1.95 g, 4 mmol), *n*-butyllithium (2.4 M, 5 mmol), and chlorotriphenylsilane (2.60 g, 5.5 mmol) were employed. Petroleum ether/dichloromethane (6:1, v/v) was used as eluent for column chromatography. The final product was a white powder (1.98 g, 74.3 %). ^{1}H NMR (400 MHz, $CDCl_3$): δ = 6.25–6.28 (m, 2 H), 6.48–6.51 (m, 2 H), 6.57–6.61 (m, 2 H), 6.89–6.93 (m, 2 H), 7.08–7.11 (m, 2 H), 7.26–7.39 (m, 11 H), 7.45–7.56 (m, 11 H), 7.75 (d, J = 7.5 Hz, 1 H), 7.80–7.82 ppm (m, 2 H); ^{13}C NMR (100 MHz, $CDCl_3$): δ = 155.46, 155.36, 141.45, 140.78, 140.00, 139.68, 136.34, 135.26, 134.24, 133.82, 133.48, 131.08, 130.88, 129.47, 128.77, 127.72, 126.99, 125.97, 125.00, 120.43, 120.25, 119.54, 114.47, 57.07 ppm; MS: *m/z*: 665.37; elemental analysis calcd (%) for $C_{49}H_{35}NSi$: C 88.38, H 5.30, N 2.10; found: C 88.25, H 5.30, N 2.30.

Acknowledgements

We acknowledge financial support from the National Science Foundation of China (Nos.61036009, 61177016, 21172162, 21202114, and 21161160446), the National High-Tech Research Development Program (No. 2011AA03A110), and the Natural Science Foundation of Jiangsu Province (No. BK2010003).

---

[1] Special issue on High Efficiency Light Emitters, *Org. Electron.* **2003**, *4*, 45–198.

[2] Special issue on π-Functional Materials, *Chem. Mater.* **2011**, *23*, 309–922.

[3] M. A. Baldo, D. F. O'Brien, Y. You, A. Shoustikov, S. Sibley, M. E. Thompson, S. R. Forrest, *Nature* **1998**, *395*, 151–154.

[4] Y. Ma, H. Zhang, J. Shen, C. Che, *Synth. Met.* **1998**, *94*, 245–248.

[5] R. C. Kwong, S. Sibley, T. Dubovoy, M. Baldo, S. R. Forrest, M. E. Thompson, *Chem. Mater.* **1999**, *11*, 3709–3713.

[6] T.-F. Guo, S.-C. Chang, Y. Yang, R. C. Kwong, M. E. Thompson, *Org. Electron.* **2000**, *1*, 15–20.

[7] C. Adachi, M. A. Baldo, S. R. Forrest, S. Lamansky, M. E. Thompson, R. C. Kwong, *Appl. Phys. Lett.* **2001**, *78*, 1622–1624.

[8] C. Adachi, M. A. Baldo, M. E. Thompson, S. R. Forrest, *J. Appl. Phys.* **2001**, *90*, 5048–5051.

[9] R. J. Holmes, B. W. D′Andrade, S. R. Forrest, X. Ren, J. Li, M. E. Thompson, *Appl. Phys. Lett.* **2003**, *83*, 3818–3820.

[10] K. Brunner, A. Van Dijken, H. Boerner, J. J. A. M. Bastiaansen, N. M. M. Kiggen, B. M. W. Langeveld, *J. Am. Chem. Soc.* **2004**, *126*, 6035–6042.

[11] A. Chaskar, H.-F. Chen, K.-T. Wong, *Adv. Mater.* **2011**, *23*, 3876–3895.

[12] Y. Tao, C. Yang, J. Qin, *Chem. Soc. Rev.* **2011**, *40*, 2943–2970.

[13] S. O. Jeon, J. Y. Lee, *J. Mater. Chem.* **2012**, *22*, 4233–4243.

[14] Z.-F. An, R.-F. Chen, J. Yin, G.-H. Xie, H.-F. Shi, T. Tsuboi, W. Huang, *Chem. Eur. J.* **2011**, *17*, 10871–10878.

[15] C. Fan, F. Zhao, P. Gan, S. Yang, T. Liu, C. Zhong, D. Ma, J. Qin, C. Yang, *Chem. Eur. J.* **2012**, *18*, 5510–5514.

[16] C. Han, G. Xie, J. Li, Z. Zhang, H. Xu, Z. Deng, Y. Zhao, P. Yan, S. Liu, *Chem. Eur. J.* **2011**, *17*, 8947–8956.

[17] C. Han, Z. Zhang, H. Xu, J. Li, Y. Zhao, P. Yan, S. Liu, *Chem. Eur. J.* **2013**, *19*, 1385–1396.

[18] C. W. Lee, J.-A. Seo, M.-S. Gong, J. Y. Lee, *Chem. Eur. J.* **2013**, *19*, 1194–1198.

[19] Y. J. Cho, J. Y. Lee, *Chem. Eur. J.* **2011**, *17*, 11415–11418.

[20] C. Han, G. Xie, H. Xu, Z. Zhang, L. Xie, Y. Zhao, S. Liu, W. Huang, *Adv. Mater.* **2011**, *23*, 2491–2496.

[21] C. Han, Z. Zhang, H. Xu, J. Li, G. Xie, R. Chen, Y. Zhao, W. Huang, *Angew. Chem. Int. Ed.* **2012**, *51*, 10104–10108.

[22] C. Han, Z. Zhang, H. Xu, S. Yue, J. Li, P. Yan, Z. Deng, Y. Zhao, P. Yan, S. Liu, *J. Am. Chem. Soc.* **2012**, *134*, 19179–19188.

[23] C. Adachi, R. C. Kwong, P. Djurovich, V. Adamovich, M. A. Baldo, M. E. Thompson, S. R. Forrest, Appl. Phys. Lett. 2001, 79, 2082–2084.

[24] X. Ren, J. Li, R. J. Holmes, P. I. Djurovich, S. R. Forrest, M. E. Thompson, *Chem. Mater.* **2004**, *16*, 4743–4747.

[25] J.-J. Lin, W.-S. Liao, H.-J. Huang, F.-I. Wu, C.-H. Cheng, *Adv. Funct. Mater.* **2008**, *18*, 485–491.

[26] M.-S. Lin, L.-C. Chi, H.-W. Chang, Y.-H. Huang, K.-C. Tien, C.-C. Chen, C.-H. Chang, C.-C. Wu, A. Chaskar, S.-H. Chou, H.-C. Ting, K.-T. Wong, Y.-H. Liu, Y. Chi, *J. Mater. Chem.* **2012**, *22*, 870–876.

[27] Y. H. Kim, H. C. Jeong, S. H. Kim, K. Yang, S. K. Kwon, *Adv. Funct. Mater.* **2005**, *15*, 1799–1805.

[28] J.-W. Kang, D.-S. Lee, H.-D. Park, J. W. Kim, W.-I. Jeong, Y.-S. Park, S.-H. Lee, K. Go, J.-S. Lee, J.-J. Kim, *Org. Electron.* **2008**, *9*, 452–460.

[29] S.-J. Yeh, M.-F. Wu, C.-T. Chen, Y.-H. Song, Y. Chi, M.-H. Ho, S.-F. Hsu, C. H. Chen, *Adv. Mater.* **2005**, *17*, 285–289.

[30] M.-H. Tsai, H.-W. Lin, H.-C. Su, T.-H. Ke, C.-c. Wu, F.-C. Fang, Y.-L. Liao, K.-T. Wong, C.-I. Wu, *Adv. Mater.* **2006**, *18*, 1216–1220.

[31] W.-S. Han, H.-J. Son, K.-R. Wee, K.-T. Min, S. Kwon, I.-H. Suh, S.-H. Choi, D. H. Jung, S. O. Kang, *J. Phys. Chem. C* **2009**, *113*, 19686–19693.

[32] Z. Jiang, Y. Chen, C. Fan, C. Yang, Q. Wang, Y. Tao, Z. Zhang, J. Qin, D. Ma, *Chem. Commun.* **2009**, 3398–3400.

[33] M.-K. Leung, W.-H. Yang, C.-N. Chuang, J.-H. Lee, C.-F. Lin, M.-K. Wei, Y.-H. Liu, *Org. Lett.* **2012**, *14*, 4986–4989.

[34] S. Gong, Y. Chen, C. Yang, C. Zhong, J. Qin, D. Ma, *Adv. Mater.* **2010**, *22*, 5370–5373.

[35] M. Kim, J. Y. Lee, *Org. Electron.* **2012**, *13*, 1245–1249.

[36] J. Zhao, G. Xie, C. Yin, L. Xie, C. Han, R. Chen, H. Xu, M. Yi, Z. Deng, S. Chen, Y. Zhao, S. Liu, W. Huang,, *Chem. Mater.* **2011**, *23*, 5331–5339.

[37] S.-C. Dong, C.-H. Gao, Z.-H. Zhang, Z.-Q. Jiang, S.-T. Lee, L. S. Liao, *Phys. Chem. Chem. Phys.* **2012**, *14*, 14224–14228.

[38] S.-C. Dong, C.-H. Gao, X.-D. Yuan, L.-S. Cui, Z.-Q. Jiang, S.-T. Lee, L.-S. Liao, *Org. Electron.* **2013**, *14*, 902–908.

[39] Z. Jiang, Z. Liu, C. Yang, C. Zhong, J. Qin, G. Yu, Y. Liu, *Adv. Funct. Mater.* **2009**, *19*, 3987–3995.

Received: March 22, 2013